Structural and electronic properties of α-tin nanocrystals from first principles

Sebastian Küfner,* Jürgen Furthmüller, Lars Matthes, Martin Fitzner, and Friedhelm Bechstedt
Institut für Festkörpertheorie und -optik, Friedrich-Schiller-Universität, and European Theoretical Spectroscopy Facility (ETSF), Max-Wien-Platz 1, 07743 Jena, Germany
(Received 27 February 2013; published 17 June 2013)

The α phase of tin is a zero-gap semiconductor with an inverted band structure with respect to other group-IV elements like Ge. The Γ_{6c} states lie energetically below the Γ_{8v} levels. How these unique electronic properties transform in nanostructures with spatial confinement has not been studied. We apply density-functional theory within the local density approximation to investigate the energetic, structural, and electronic properties of bulk α-Sn and its nanocrystals (NCs) up to a size of 363 Sn atoms. For NCs with larger diameters up to 14 nm the tight-binding method is applied for the electronic states. Spin-orbit coupling is taken into account. The clusters are modeled in such a way that the T_d symmetry of the bulk system is conserved. Their surfaces are passivated with hydrogen. We show that the spatial confinement causes not only a decrease of the fundamental gap for increased NC size but also a topological transition where the ordering of s- and p-like highest-occupied molecular orbital and lowest-unoccupied molecular orbital states is interchanged. The influence of quasiparticle and excitonic effects on the lowest pair excitation energies is investigated within approximations based on the hybrid exchange-correlation functional by J. Heyd, G. E. Scuseria, and M. Ernzerhof [J. Chem. Phys. **118**, 8207 (2003)] (HSE) and the ΔSCF method.

DOI: 10.1103/PhysRevB.87.235307 PACS number(s): 61.46.Hk, 71.20.Mq, 71.70.Ej, 81.05.Cy

I. INTRODUCTION

Nanostructuring significantly changes the behavior of a crystalline material.[1,2] This is caused mainly by two effects: the quantum confinement and the surface. When the size of a nanostructure becomes smaller than characteristic lengths of the bulk material such as the exciton radius, the Fermi wavelength, or the Thomas-Fermi screening length the physical and chemical properties are drastically modified. Then manipulation of electronic and optical properties are possible by controlling their size. In addition, due to the increasing surface/volume ratio with decreasing size, surface geometry and chemistry play an important role. For instance, the tendency to minimize the surface energy causes structural relaxations inside a nanostructure.[3,4] Moreover, different surface passivations and matrix materials influence the resulting properties.[5]

Interesting systems to study the influence of nanostructuring are zero-gap semiconductors such as α-Sn and HgTe[6] with an inverted band structure where the fourfold degenerated Γ_{8v} states are energetically equivalent to the Fermi level. Because of the relativistic mass-Darwin effect, the s-like Γ_{6c} levels are energetically lower than the p-like Γ_{8v} levels and hence form an inverted band structure with a "negative gap" compared to other group-IV semiconductors like germanium or compound semiconductors such as CdTe.[6,7]

For nanostructures, in particular in form of nanocrystals (NCs), however, widely tunable narrow band gap energies and tunable strong infrared emissions have been predicted or observed.[8–10] Nevertheless, in general, less is known about the properties of nanocrystals made by zero-gap semiconductors, in particular α-Sn, from theoretical as well as experimental studies. This is astonishing when the situation is compared with that for other group-IV-based NCs. Many theoretical, especially *ab initio* studies exist for Si and Ge NCs (see Refs. 11–13 and references therein) but not for α-Sn particles. One challenge for all theoretical studies is the inclusion of the strong spin-orbit coupling (SOC). From an experimental point of view, some difficulties occur when preparing Sn nanocrystals with tedrahedrally coordinated bonding geometries. Bulk elemental tin possesses two allotropes. Besides the semimetallic tetragonal β-Sn structure under ambient conditions, there exists a cubic semiconducting α-Sn for temperatures below 13.2 °C.[6,14–16] It has the same tedrahedral diamond lattice as Si and Ge. In amorphous materials, e.g., SiO_2 or Si_3N_4, usually Sn NCs are prepared with the β structure.[17,18] However, crystalline matrices such as Si and Ge prevent the collapse to the denser β form and particles of α-Sn can be stabilized.[19–22]

For zero-dimensional nanostructures in general but for α-Sn NCs above all there are several unsolved problems which are basically related to the scalar-relativistic and spin-orbit effects. For NCs with small diameters a gap opening is expected due to carrier confinement. With rising NC size, however, the s-like Γ_{6c} bulk level should dip below the p-like Γ_{8v} level leading to the band inversion known for bulk α-Sn. It has been pointed out[23,24] that when such band inversion occurs at time-reversal invariant wave vectors, it produces peculiar electronic properties such as Dirac cones in the fundamental energy gap. Despite the fact that no translational invariance appears for NCs, band (or level) inversion should happen for a finite diameter. The value of this diameter is unknown. In any case, the change from normal band ordering to band inversion may be called "topological" transition in agreement with the identification of α-Sn as a topological semimetal.[25] The second open problem is the influence of the nanocrystal, especially its surface and its surface passivation on the spin-orbit splitting of the Γ_7 and Γ_8 states. In typical tight-binding calculations of α-Sn and also HgTe NCs one only considers a constant, size-independent intra-atomic term of the spin-orbit coupling of the atomlike p orbitals.[8,26,27]

In the present work we apply *ab initio* calculational methods to investigate the geometry and electronic structure of α-Sn nanocrystals. For purpose of comparison and the possibility to

extend the electronic-structure studies towards NC diameters of about 14 nm we also apply the tight-binding method.[28] In order to test the first-principles method for both properties, structure and electronic states, as well as the tight-binding method for the electronic structure and to demonstrate their reliability, the first part of the paper deals with α-Sn bulk. In a second step the methods are applied to α-Sn NCs. In Sec. II the theoretical and computational methods are described. In the subsequent Sec. III we apply several computational approaches to bulk α-Sn, especially for the electronic structure. The band ordering as well as the SOC of valence p-derived states is studied. The results of the different methods for hydrogenated α-Sn nanocrystals are presented in Sec. IV. We investigate the energetics, the geometry, and the electronic structure including SOC. The size dependence of the fundamental gap and its inversion for larger diameters are discussed in particular. Finally, in Sec. V a summary and conclusions are given.

II. THEORETICAL AND COMPUTATIONAL METHODS

A. First-principles methods

We apply the density functional theory (DFT)[29] within the local density approximation (LDA)[30] implemented in the Vienna *ab initio* simulation package (VASP).[31,32] Exchange and correlation are treated using the quantum Monte Carlo results of Ceperly and Alder[33] as parametrized by Perdew and Zunger.[34] In order to study the influence of exchange and correlation (XC) on the band structure in the bulk case, we further apply gradient corrections using the generalized gradient approximation (GGA)[35–37] and the LDA + U method[38] that takes an additional intra-atomic Coulomb interaction U into account.[3] Band-structure calculations are also performed using hybrid XC functional HSE06 containing a fraction of short-range nonlocal Fock exchange.[39] In this way the well-known problem of a significant underestimation of fundamental energy gaps in DFT-LDA and DFT-GGA[40] is removed. Nevertheless, the resulting quasiparticle gaps do not correctly describe the lowest electron-hole pair energies measured in optical spectroscopies due to the exclusion of excitonic effects. In zero-dimensional nanostructures with electronic confinement in all spatial directions optical gaps including quasiparticle and excitonic effects are computed using the δ self-consistent field (ΔSCF) method,[41] its reliability has been demonstrated for colloidal and embedded nanocrystals.[5,42–44] It is based on an excited-state calculation within the DFT using an occupation constraint. One electron is taken from the highest occupied molecular orbital (HOMO) and placed into the lowest unoccupied molecular orbital (LUMO). The HOMO is assumed to remain unoccupied minimizing the total energy. In the case of orbital degeneracy an average over the HOMO and LUMO states is considered.

The electron-ion interaction is described by pseudopotentials that are generated within the projector-augmented wave (PAW)[45,46] method. All calculations, including structural optimizations, are performed including scalar-relativistic effects and spin-orbit coupling.[47] The Sn 4d, Sn 5s, and Sn 5p electrons are treated as valence electrons in bulk calculations. However, we show that the Sn 4d electrons have no major impact on the electronic structure of the NCs and, hence, in order to keep the computational effort on a sustainable level, we neglect the d electrons for the structural optimization and the electronic structure of the largest NCs studied within the described *ab initio* framework. The electronic states in-between the PAW spheres are expanded into a plane-wave basis set with an energy cutoff of 500 eV for bulk calculations and 200 to 300 eV for the nanocrystals, depending on the NC size. In case of α-Sn bulk, Brillouin zone (BZ) integrations are replaced by a sum over $12\times12\times12$ Monkhorst-Pack[48] $\mathbf{k}$ points. However, as no $\mathbf{k}$ dispersion is expected for NCs because of the huge unit cells in real space, we only consider the Γ point in NC studies. Structural relaxation is performed applying a conjugated-gradient algorithm minimizing the forces acting on the atoms. The optimized lattice constant of α-tin and the atomic positions in the nanocrystals are determined, ensuring that the Hellmann-Feynman forces acting on the atoms are well below 5 and 20 meV/Å, respectively. Within each atomic relaxation step, the electronic structure is converged such that the total energy difference is smaller than 10^{-5} eV.

B. Tight-binding description

The *ab initio* treatment of nanostructures is restricted to numbers of Sn atoms below 600. In order to also treat the electronic structure of much larger nanocrystals up to 20 000 Sn atoms we use a tight-binding (TB) model of α-Sn which gives excellent agreement with the approximate quasiparticle band structure computed within the HSE + SOC framework and displayed in Fig. 2. Existing TB parametrizations are not sufficiently accurate compared with an HSE + SOC band structure. Usually SOC is ignored.[28,49,50] The model of Pedersen *et al.*[51] takes nonorthogonality of the TB orbitals and third-nearest-neighbor interaction into account and, hence, its handling for big nanocrystals is difficult. We develop our own TB parametrization for the electronic structure calculations. Details are described in the Appendix. The TB Hamiltonian matrix is written in a basis of atomic orbitals. We widely follow the idea of Vogl *et al.*[28] We apply an sp^3s^* basis set and restrict the intersections to nearest-neighbor atoms. However, two extensions are taken into account, the spin-orbit interaction and three-center integral $A = 1.995$ eV modeling pp interactions in addition to two-center integrals. Thereby we follow an idea of Li and Lin-Chung.[52] The inclusion of SOC requires a doubling of the basis set. As usual in TB approaches[53] we only consider the intra-atomic terms of the spin-orbit coupling on the p orbitals leading to a $\Gamma_{8v} - \Gamma_{7v}$ splitting of $\Delta_0 = 0.68$ eV. Inter-atomic terms which give rise to a Rashba or Dresselhaus splitting of the p-derived bands away from Γ[54] are neglected. The two-center integrals and the diagonal intra-atomic terms are obtained by a fitting procedure to the HSE + SOC eigenvalues at the high-symmetry points Γ, X, and L shown in Fig. 2. A simple procedure is applied to minimize the average deviation of the HSE + SOC and TB + SOC eigenvalues. The resulting TB parameters are listed in Table III in the Appendix. For the hydrogen passivation of the NCs, we use a basis of one hydrogen s orbital yielding four Sn-H matrix elements between the H s and the Sn sp^3s^* basis orbitals and one matrix element for the hydrogen s self-interaction. We neglect the ss^* interaction in accordance to Vogl *et al.*[28]

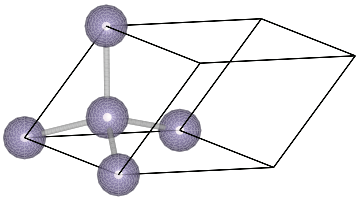

FIG. 1. (Color online) Primitive unit cell and atomic positions of bulk α-Sn.

III. BULK α-Tin

A. Structure and energetics

The α phase of tin crystallizes in the diamond structure [space group $O_h^7(Fd3m)$] with a face-centered-cubic Bravais lattice and two atoms in the unit cell located at (0,0,0) and (0.25,0.25,0.25) in units of the crystal axes.[16] Each atom is tedrahedrally coordinated by four neighboring atoms giving a local T_d symmetry. The unit cell and the atomic positions are displayed in Fig. 1. Computed parameters that characterize structural, energetic, and elastic properties are listed and compared to experimental values in Table I. We calculate the lattice constant to be $a_0 = 6.4746$ Å, which is in excellent agreement with the values measured by Farrow[55] and Davey[56] using x-ray diffraction. A slight underestimation of 5 mÅ (Ref. 55) and 15 mÅ (Ref. 56), respectively, within DFT-LDA can be explained by the well-known tendency of the LDA to underestimate bond lengths.[35] The calculated bulk modulus $B_0 = 44.8$ GPa is in rather good agreement with the measured values.[57,58] Other DFT-LDA values $a_0 = 6.479$ or 6.406 Å[17,51] deviate much more from experimental values, while the computed bulk modulus $B_0 = 45$ GPa[51] is very similar to our value. Using the DFT-GGA description with the PBE exchange-correlation functional,[37] larger lattice constants $a_0 = 6.656$, 6.654, and 6.663 Å[59,60] have been found. The corresponding bulk modulus $B_0 = 36.0$, 36.3, or 35.9 GPa[59,60] is pretty much underestimated.

The cohesive energy $E_{\rm coh}$ is calculated as the difference between the total energy per tin atom in the bulk $E_{\rm bulk}^{\alpha\text{-Sn}} = -4.482$ eV and the total energy of the free tin atom in its spin-polarized ground state. The modification of the total energy of the free atom due to the spin-orbit interaction was calculated to be $E_{\rm Sn} = -0.375$ eV using orthorhombic supercells with edge lengths of $15 \times 16 \times 17$ Å. The resulting cohesive energy is $E_{\rm coh} = 4.11$ eV. This value is somewhat larger than the experimental value $E_{\rm coh}^{\rm expt} = 3.12$ eV.[58]

TABLE I. The lattice constant a_0, the bulk modulus B_0 (in GPa), its pressure derivative B_0', the total energy $E_{\rm bulk}^{\alpha\text{-Sn}}$, and the cohesive energy $E_{\rm coh}$ (in eV) per formula unit (f.u.).

	a_0 (Å)	B_0 (GPa)	B_0'	$E_{\rm bulk}^{\alpha\text{-Sn}}$ (eV)	$E_{\rm coh}$ (eV)
This work (LDA)	6.4746	44.8	4.85	−4.482	4.11
Expt.	6.4798,[a] 6.4892[b]	53.1[c]			3.12[d]

[a]Reference 55.
[b]Value cited in Ref. 56.
[c]Reference 16.
[d]Reference 58.

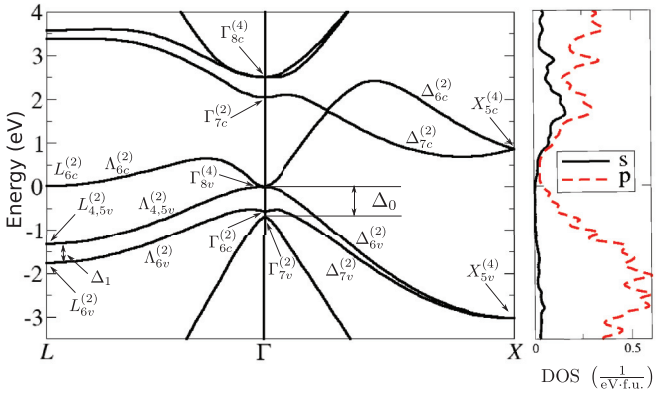

FIG. 2. (Color online) Band structure of α-Sn calculated using SOC and the hybrid functional HSE06.[46] Additionally, the angular-momentum resolved DOS is given to describe the symmetry of the electronic states in a certain energy interval. The irreducible representations and their degeneracy are indicated. The Γ_{8v} level is used as energy zero.

B. Electronic structure

The quasiparticle band structure and the density of states (DOS) resulting from the generalized Kohn-Sham eigenvalues obtained with the HSE hybrid exchange-correlation functional and spin-orbit interaction are presented in Fig. 2. We observe the well-known result: α-Sn is a zero-gap semiconductor[6] or topological semimetal[25] with an inverted band structure with respect to other group-IV semiconductors like silicon and germanium.[16,25,57,61–64] For germanium, the lowest conduction band at Γ is s derived and has Γ_{6c} symmetry, while the highest valence bands are p derived and therefore transform like Γ_{7v} and Γ_{8v}. In the case of α-Sn, this energetic ordering of the bands is inverted leading to a "negative gap" $-E_g$.[16,25,57,61–64] As can be seen in Fig. 2, the s-like Γ_{6c} states are energetically lower than the p-like Γ_{8v} levels but still above the spin-orbit splitted Γ_{7v} level. However, the energetic ordering of Γ_{7v} and Γ_{6c} is under debate in the literature and seems to depend on the calculational method. Test calculations within LDA, GGA, and LDA + U result in a Γ_{7v} level to be above Γ_{6c} (see Table II) which is in accordance with $\mathbf{k}\cdot\mathbf{p}$ calculations by Cardona *et al.*[62,63] However, using the HSE06 functional which takes partially into account the nonlocal Fock exchange, we determine Γ_{6c} to be 100 meV higher in energy than Γ_{7v}. The band ordering $\Gamma_{7v} < \Gamma_{6c} < \Gamma_{8v}$ and the level distances are almost in agreement with recent quasiparticle calculations within Hedin's GW approximation.[65,66] This result also agrees with the tight-binding calculations by Chadi,[53] while empirical

TABLE II. The calculated spin-orbit splittings Δ_0 and Δ_1, negative gaps $-E_g$, and binding energies of the d-states E_d within different approximations for exchange and correlation. All values in eV.

Method	Δ_0 (eV)	Δ_1 (eV)	$-E_g$	E_d (eV)
LDA	0.691	0.439	1.053	21.13
GGA	0.666	0.424	0.831	21.02
LDA + U	0.661	0.439	0.852	24.00
HSE	0.681	0.437	0.519	23.30

pseudopotential calculations yield the same band ordering $\Gamma_{8v} > \Gamma_{6c} > \Gamma_{7v}$ but an increased $\Gamma_{6c} - \Gamma_{7v}$ distance up to 0.38 eV.[7] Interestingly the different treatments of exchange and correlation mainly affect the negative fundamental gap $E_g = \Gamma_{6c} - \Gamma_{8v}$, while the spin-orbit splitting constants $\Delta_0 = \Gamma_{8v} - \Gamma_{7v}$ and $\Delta_1 = L_{4,5v} - L_{6v}$ are rather independent of the used LDA, GGA, LDA + U, and HSE functionals. As a consequence the band ordering $\Gamma_{6c} > \Gamma_{7v}$ is interchanged to $\Gamma_{7v} > \Gamma_{6c}$ in all local or semilocal treatments of XC (see Table II).

The XC functional also influences the binding energy E_d of the Sn 4d electrons (see Table II). According to the pd repulsion in diamond and zinc-blende structure crystals[67] smaller binding energies are usually related to a stronger repulsion of the p-type valence band maximum and, hence, to a reduction of the fundamental sp gap E_g.[68] Here, in the case of α-Sn with a negative gap, the situation is less clear for the absolute gap value. Nevertheless, going from LDA with a smaller binding energy of the d electrons to LDA + U or HSE with larger binding energies the absolute gap value decreases in agreement with the position of the Γ_{6c} level below the Γ_{8v} one.

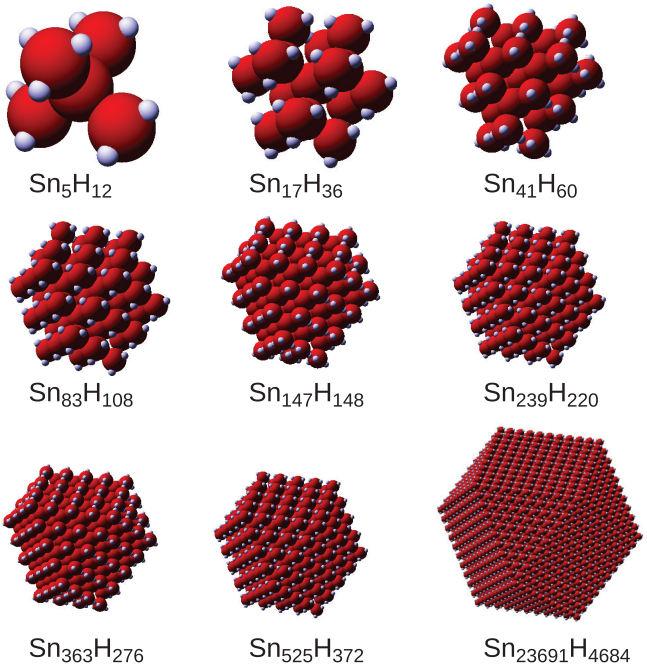

FIG. 3. (Color online) Atomic geometries of the studied nanocrystals. Tin atoms are marked by large red spheres, while the passivating hydrogen atoms are represented by small white dots. The resulting {001} and {111} facets are clearly visible.

IV. α-TIN NANOCRYSTALS

A. Geometry

In order to simulate the structural, energetic, and electronic properties of isolated α-Sn NCs, we use simple cubic supercells with the central NC atom placed in the center of the supercell. The Sn NCs are constructed assuming fourfold coordination of each atom as in bulk α-Sn. The construction starts with a central atom and adds tin atoms shell by shell, thereby keeping the local tedrahedral symmetry.[69] The geometry of the NCs conserves the point-group symmetry T_d of the bulk system. The edge length of the supercells is determined in such a way that the resulting electron bands can be described by dispersionless levels. The resulting NC shape corresponds to a cubo-octahedron as illustrated in Fig. 3. The NCs represent cubes with (001) surfaces whose corners are cut perpendicular to ⟨111⟩ directions, and, hence, form triangular faces that connect the midpoints of the rectangulars at the respective corners. The resulting NC surfaces exhibit six rectangular {001} and eight equilateral triangular {111} facets and contain $N_{Sn} = 1$, 5, 17, 41, 83, 147, 239, 363, and 525 tin atoms that are treated from first principles. The shape of the facets shows an alternating behavior with respect to the number of shells. The dots with 17, 83, 239, and 525 atoms exhibit square {001} facets. In this case, all {111} facets have the same size. On the other hand, in case of 41, 147, and 363 tin atoms, the {001} facets are rectangular and the two sides of a rectangle differ by one atom. Hence, in this case, there are two different {111} facets with edge lengths equal to the two different edges of such a rectangular {001} facet. The average distance of the outermost Sn atoms to the NC center is considered as the nominal NC radius. The atoms on {001} facets possess two dangling bonds, whereas {111} ones only show one dangling bond per atom. However, in some cases atoms on the edges between two differently orientated facets exhibit three dangling bonds. Dangling bonds at the NC surface are passivated with $N_H = 4$, 12, 36, 60, 108, 148, 220, 276, and 372 hydrogen atoms in such a way that a hydrogen atom is positioned in the direction of a dangling bond at a distance of 1.73 Å, the sum of the two covalent radii.[70] The passivation shifts surface dangling bond states out of the energetic range of the fundamental energy gap as shown by Luo *et al.*[71]

In order to study the electronic structure of larger NCs in the framework of the TB approximation, the described construction principle is applied to larger NCs until 25 Sn shells, i.e., until a NC with 19 335 Sn atoms and 4092 H atoms resulting in a maximum NC diameter of 13.2 nm. However, for the larger NCs the Sn-Sn bond length is fixed to its bulk value $d = 2.804$ Å. Figure 3 shows some of the resulting structures.

The geometries of nanocrystals up to $Sn_{525}H_{372}$ with nine Sn shells and a nominal diameter of 4 nm are fully optimized by means of the *ab initio* methods described in Sec. II. In the case of the smaller NCs Sn_1H_4, Sn_5H_{12}, $Sn_{17}H_{36}$, $Sn_{41}H_{60}$, $Sn_{83}H_{108}$, and $Sn_{147}H_{148}$ the Sn 4d electrons and the spin-orbit interaction have been taken into account. However, we realized that their influence is negligibly small in agreement with the large Sn 4d binding energy (Table II) and earlier observations of a negligible influence of SOC on the structural properties up to elements of the sixth row of the Periodic Table.[60] In the case of NCs with intermediate sizes, $Sn_{239}H_{220}$, $Sn_{363}H_{276}$, and $Sn_{525}H_{372}$, only Sn 5s and Sn 5p electrons are considered as valence electrons in the first-principles calculations.

The atomic relaxation changes the bond lengths of the NCs compared to the bulk value with the constraint of conservation of the T_d symmetry. As a result the radially averaged Sn-Sn bond lengths are plotted versus the distance of the middle of the bond from the NC center in Fig. 4(a). The values in the NC cores are larger than the bulk value $d = 2.804$ Å

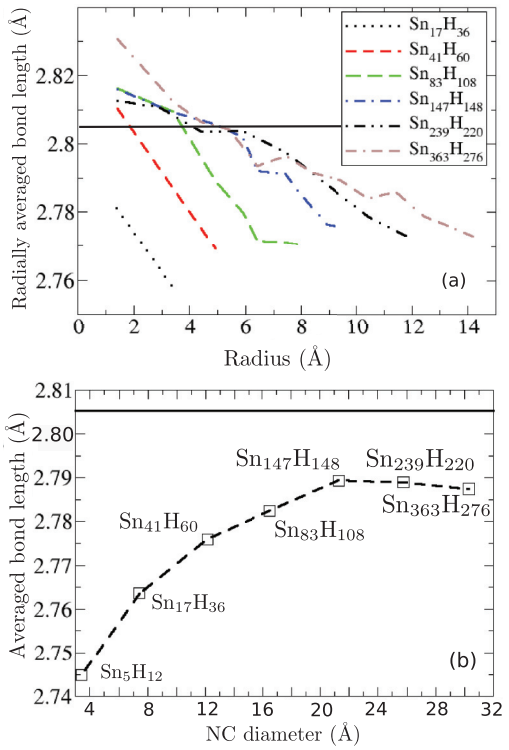

FIG. 4. (Color online) (a) Radially averaged bond length versus the bond distance to the NC center and (b) globally averaged bond length depending on the NC diameter. The horizontal solid lines indicate the bulk bond length.

approaching a maximum value for the center bonds. They decrease toward the NC surface. For distances above the half nominal NC radius the local bond lengths are even smaller than the bulk value. As a consequence we state tensile strain near the NC center but compressive strain near the surface of the NCs. These findings are very similar to those found for other group-IV nanocrystals.[5,44,69,72] The contraction of the bonds can be traced back to surface stress effects known for spherical drops,[73] while the expansion may be a consequence of the additional degrees of freedom compared to the bulk situation.

The net result for all Sn-Sn bonds is displayed in Fig. 4(b). It shows the average bond length for each NC versus its nominal diameter. There is an increase of the averaged bond lengths with increasing NC diameter. For the NCs until diameters of 4 nm the average bond length remains however smaller than the corresponding bulk value. For a $Sn_{83}H_{108}$ NC with a nominal diameter of 2.1 nm the average bond length is still 0.6% shorter than the bulk one. This deviation should be reduced with rising NC size. The slight decrease for the largest dots in Fig. 4(b) is probably a result of the larger Hellmann-Feynman forces that are allowed as breaking-out criterion of the relaxation for computational reasons. The lower average bond lengths of the NCs with respect to the bulk is caused by the tendency to lower the surface energy and the resulting inward relaxation of the outermost atoms. However, for a further increase of the NC diameter the averaged bond length should converge toward the bulk value.

The average bond length between an outermost Sn atom and a passivating hydrogen atom increases from 1.707 Å for the SnH_4 NC to 1.736 Å for $Sn_{363}H_{276}$. The shortest Sn-H bonds differ by approximately 20 mÅ from the average value in case of $Sn_{363}H_{276}$. However, this difference increases approximately linearly with the NC size.

B. Enthalpy of formation

To study the energetic stability of the NCs with N_{Sn} tin atoms and N_H passivating hydrogen atoms, we calculate their formation energy or enthalpy of formation ΔH_f as difference

$$\Delta H_f = E_{NC}(N_{Sn}, N_H) - N_{Sn} \cdot \mu_{Sn} - N_H \cdot \mu_H, \qquad (1)$$

where $E_{NC}(N_{Sn}, N_H)$ is the total DFT ground-state energy (including ion-ion repulsion) of the NC and the chemical potentials μ_{Sn} and μ_H of the particle reservoirs per atom. The preparation conditions of the NCs can be nearly modeled by the choice of the chemical potentials. In the case of the Sn reservoir we allow for a significant variation of μ_{Sn}. The upper bound $\mu_{Sn}^{bulk} = E_{bulk}^{\alpha\text{-Sn}}$ simulates Sn-rich preparation conditions where solid α-tin acts as reservoir. Deviations $\Delta\mu_{Sn} = \mu_{Sn} - \mu_{Sn}^{bulk}$ from the bulk value with

$$-\infty < \Delta\mu_{Sn} \leqslant 0 \qquad (2)$$

allow us to also model Sn-poor conditions. For the hydrogen reservoir in the preparation process we study two special situations. One possibility is the use of molecular hydrogen for passivation, i.e., $\mu_H = \frac{1}{2}\mu_{H_2} = -\frac{1}{2}E_{mol}^{H_2}$ with the binding energy of a H_2 molecule, $E_{mol}^{H_2} = 6.7$ eV, as calculated in DFT-LDA. Another possibility is that a gas of SnH_4 (tin hydride = stannane) molecules acts as reservoir. In this case, it holds $\mu_H = \frac{1}{4}[E_{NC}(1,4) - \mu_{Sn}]$ with the binding energy $-E_{NC}(1,4) = 16.53$ eV of a SnH_4 molecule.

Results are illustrated in Fig. 5. For NC passivation by means of H_2 molecules the enthalpies of formation per Sn atom in Fig. 5(a) increase for Sn-poor preparation conditions but take the smallest values for Sn-rich conditions $\mu_{Sn} = \mu_{Sn}^{bulk}$. The dependence on the chemical potential is linear in accordance with Eq. (1). The largest formation energy is observed for the smallest NC SnH_4, while it vanishes toward bulk α-Sn. The effect of the NC size on the enthalpy of formation is better represented in Fig. 5(b). The upper bound of Sn-rich preparation conditions $\mu_{Sn} = \mu_{Sn}^{bulk}$ is applied for the simulation. The formation energy vanishes for large NC diameters, thereby indicating some Ostwald ripening if diffusion of Sn atoms is possible. For small NC diameters the situation is totally different. For the smallest nanocrystal SnH_4 one derives $\Delta H_f = E_{NC}(1,4) - E_{bulk}^{\alpha\text{-Sn}} - 2E_{mol}^{H_2} = 1.35$ eV, the formation energy of SnH_4 from solid tin and molecular hydrogen, which is energetically unfavorable. The opposite reaction, the decay of SnH_4 into bulk Sn and molecular hydrogen, is possible. For $\mu_H = \frac{1}{4}[E_{NC}(1,4) - E_{bulk}^{\alpha\text{-Sn}}]$ and $\mu_{Sn} = E_{bulk}^{\alpha\text{-Sn}}$ it holds $\Delta H_f = 0$. The different behavior of the NC formation energy for different chemical potentials of hydrogen indicates a strong influence of the preparation conditions on the energetic stability and the formation of small hydrogenated Sn nanocrystals. The preparation with a gas of

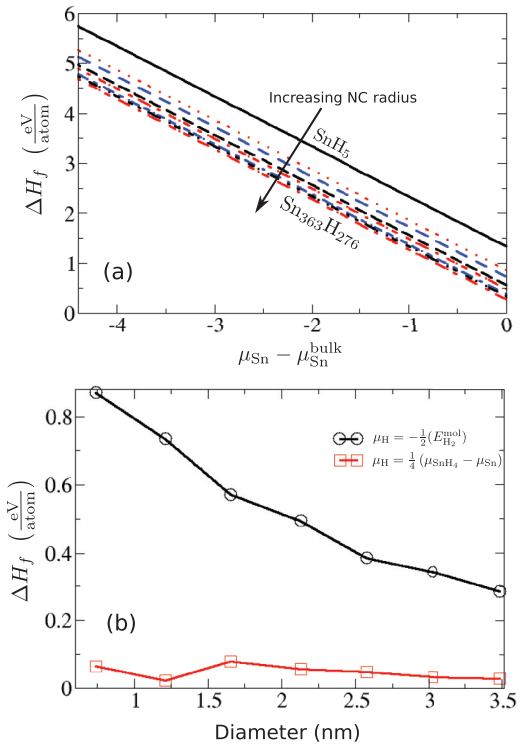

FIG. 5. (Color online) Enthalpy of formation (a) depending on the chemical potential of the tin reservoir for a H_2 gas as the hydrogen reservoir or (b) on the NC diameter for Sn-rich preparation conditions for the two choices of the hydrogen reservoir.

tin hydride molecules seems to be more favorable than the use of a gas of hydrogen molecules as a hydrogen reservoir.

C. Electronic structure

An overview over the allowed energy levels in nanocrystals up to $Sn_{525}H_{372}$, i.e., a nominal diameter of 4 nm, is given in Fig. 6, where the Kohn-Sham eigenvalues of the DFT-LDA have been used. The zeros of the energy scales have been aligned by the energy of the vacuum level of the electrostatic potential (consisting of local electron-ion attraction and Hartree potential) averaged over all space directions outside the NC. The quantum confinement effects on the energy levels are clearly visible. The fundamental gaps between HOMO and LUMO decrease with rising NC size, while the density of energy levels in the regions of empty and occupied states increases toward the high density of states in α-Sn bulk.

Most interesting is the comparison of the level ordering in the NCs with that of the bulk crystal. For illustration we study the density of states of the $Sn_{17}H_{36}$ NC and the position of its energy levels around the fundamental gap in Fig. 7. Results for other NCs are not displayed because they exhibit a similar angular-momentum resolved DOS of the HOMO and LUMO states. In Fig. 7 it is remarkable that the LUMO is mainly formed by Sn $5s$ states while Sn $4p$ states give the main contributions to the HOMO states. The contributions of states formed by the passivating hydrogen atoms in the range of the fundamental gap are significantly smaller than those of Sn s (LUMO) and Sn p (HOMO) states. The d contribution to all states around the gap remains small in agreement with

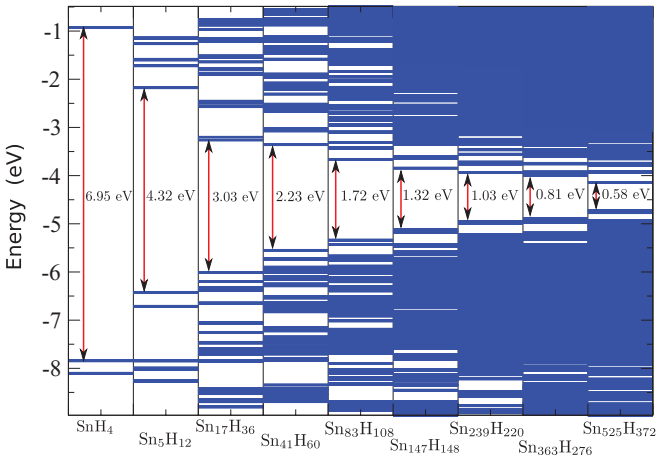

FIG. 6. (Color online) Energy-level schemes of Kohn-Sham eigenvalues of α-Sn nanocrystals passivated with hydrogen. The fundamental energy gaps are indicated by the corresponding energy eigenvalues. The energy scales of the different NCs have been aligned by the vacuum levels derived from the spatially averaged electrostatic potentials.

the discussion in Sec. III B. The strongest influence of Sn $4d$ states has been found for $Sn_{41}H_{60}$ where both HOMO and LUMO levels are shifted by 50 meV toward higher energies. As a result we state an inversion of the orbital symmetry of the electronic states around the gap with respect to the Γ_{6c} and Γ_{8v} states of bulk α-tin. However, the projections of the NC wave functions on angular-momentum eigenstates are not sufficient for the identification of the corresponding bulk states.[71,74] In order to identify the Γ_{8v}, Γ_{6c}, or Γ_{7v} character of the bulk states near the Fermi level in the NC orbitals, we apply a more appropriate projection technique.[71,75] The probability to find a bulk symmetry in a NC state is determined by evaluating the overlap

$$P(n,m,\mathbf{k}) = \sum_{i=n}^{n+d_{NC}} \sum_{j=m}^{m+d_B} \left| \int d^3\mathbf{r}\psi_i(\mathbf{r})\left[\phi_j^{\mathbf{k}}(\mathbf{r})\right]^* \right|^2 \qquad (3)$$

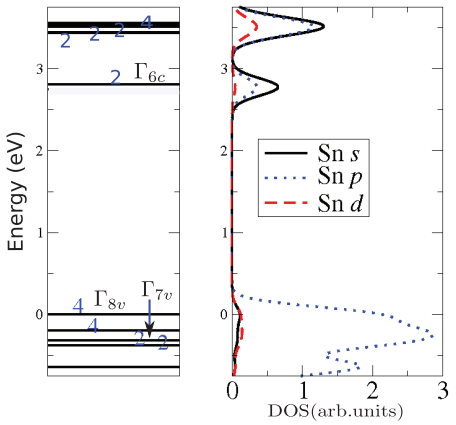

FIG. 7. (Color online) Energy levels and angular-momentum resolved density of states of the $Sn_{17}H_{36}$ NC around the fundamental gap. The bulk states that form the HOMO, LUMO, and the first occupied spin-orbit split-off NC state are labeled. The level degeneracy is indicated by numbers 2 and 4.

of the nanocrystal wave functions $\psi_n(\mathbf{r})$ and the bulk Bloch states $\phi_m^{\mathbf{k}}(\mathbf{r})$. Here n and m indicate the eigenvalue, $\mathbf{k}$ is the respective $\mathbf{k}$ point in the bulk BZ, and $\mathbf{r}$ denotes the position vector. Energetically degenerated states are summed up over the degree of degeneracy d_{NC} (d_B) of the NC (bulk) once the overlap integral has been evaluated. The results for a $Sn_{17}H_{36}$ NC in Fig. 7 show clearly that there is indeed an inversion of the level ordering around the gap. The overlap between the HOMO (LUMO) state of the NC with the Γ_{8v} (Γ_{6c}) bulk state at $\mathbf{k} = 0$ is of the order of magnitude of one, whereas all other combinations of HOMO, HOMO-1, LUMO with Γ_{8v}, Γ_{6c}, Γ_{7v}, Γ_{7c} bulk states are zero. Hence, the NC states are formed by defined bulk states, whereas the effect of coupling of multiple bulk bands is negligible. We obtained the same result applying this projection technique within the tight-binding method. Using a similar projection technique similar results concerning the dominating Γ_{6c} bulk states have been found for the HOMOS of colloidal InAs, InP, CdSe, and Si NCs.[71]

Another interesting point is the level degeneracy. Around the HOMO-LUMO gap only fourfold and twofold states appear in Fig. 7. This is a consequence of the presence of spin-orbit interaction and has been already observed for bulk α-Sn. The five ordinary representations of the T_d group, Γ_1, Γ_2, Γ_{12}, Γ_{15}, and Γ_{25}, multiplied with the representation $D_{1/2}$ of the full rotation group to account for the spinor character split into twofold degenerate Γ_6 and Γ_7 states or fourfold degenerate Γ_8 states.[76] The splitting of the uppermost occupied levels in Fig. 7 into fourfold and twofold degenerate levels is due to SOC as has been demonstrated by comparison with electronic-structure results omitting SOC (not shown here) as well as by the identification of the contributing bulk states Γ_{8v} and Γ_{7v} calculating the overlap integrals (3) between NC and bulk states.

Besides the atomic orbital symmetry of the HOMO and LUMO state the general distribution of the wave functions over the NCs is of special interest. Corresponding wave function squares are displayed in Fig. 8 using two different representations only for a small NC, Sn_5H_{12}, in order to visualize the relation to the atomic geometry. Figure 8 shows isosurfaces (left panels) of the wave function squares and the radial dependence of the wave function squares averaged over all space directions, i.e., the envelope function[12] (right panels) for the HOMO and the LUMO. The isosurface of the HOMO [Fig. 8(a)] exhibits the shape of a distorted tedrahedron according to the tedrahedral structure of the Sn NCs. It is only slightly modified by the probability to find a hole in the region of the passivating hydrogen atoms. Consequently, a dominant peak occurs in the radial probability distribution closer to the NC core. The second peak near the surface of the NC is localized at the passivating hydrogen atoms. The radial distribution of the LUMO shows quite similar behavior [see Fig. 8(b)]. However, two nodes appear. The wave function square shows that the first peak originates from a spherical isosurface around the central Sn atom. The second, more broadened peak with lower intensity results from probabilities that are located at the Sn-Sn bonds. As for the HOMO, there is also some probability to find an electron in the region of the passivating hydrogen atoms. The envelope wave functions for HOMO and LUMO of the small Sn_5H_{12} NC are similar to the radial parts of the lowest s- and p-like states of hydrogenlike ions.

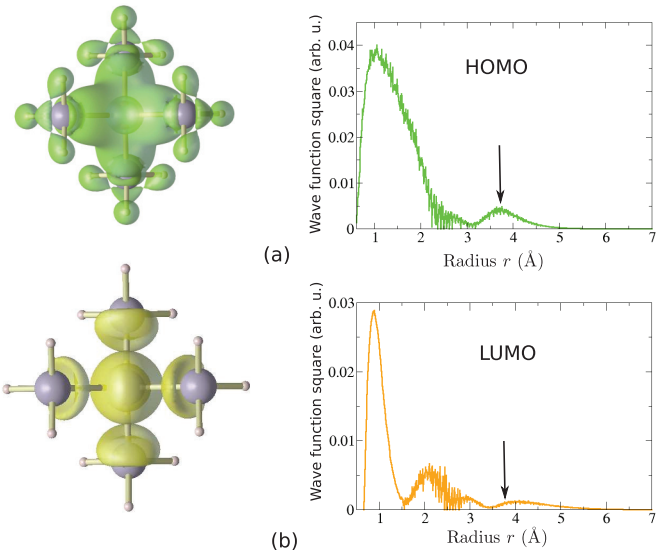

FIG. 8. (Color online) Isosurfaces of probabilities to find holes or electrons (left panels) and radially averaged wave function squares (right panels) of the (a) HOMO and for the (b) LUMO for the Sn_5H_{12} cluster. The arrow indicates the nominal radius of the NC.

The question arises how the fundamental HOMO-LUMO gaps that are depicted in Fig. 6 relate to measurable ones, for example, measured by means of optical absorption, luminescence, or scanning tunneling spectroscopy. It is well known that the Kohn-Sham (KS) energy gaps computed in the DFT-LDA framework significantly underestimate the quasiparticle gaps by 25% –100%.[40] In order to understand the influence of the excitation of electrons and holes on the fundamental gap, we study the lowest electron-hole pair excitation energies in α-Sn NCs within three different approximations for exchange and correlation using the local LDA or nonlocal hybrid HSE functional and the ΔSCF method including spin-orbit interaction. The results are summarized in Fig. 9. The lowest pair excitation energies are derived as KS eigenvalue differences between HOMO and LUMO. There is a continuous decrease

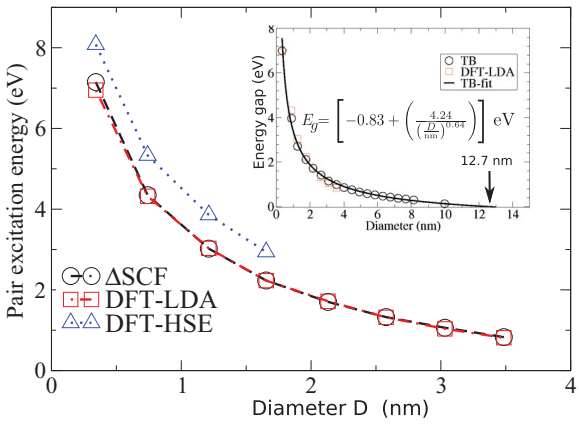

FIG. 9. (Color online) Lowest pair excitation energies of the hydrogenated Sn nanocrystals from three different *ab initio* approximations. The insert displays the HOMO-LUMO gaps taken from the TB calculations. The agreement with the DFT-LDA values is shown for small NC diameters.

from SnH_4 with about 7 eV to $Sn_{525}H_{372}$ with a gap below 0.6 eV. Both excitonic effects as well as quasiparticle effects are neglected within DFT-LDA. The use of the hybrid HSE06 functional allows us to model a substantial part of the quasiparticle corrections.[77,78] The nonlocality of the XC self-energy is taken into account. Also some of the screening reaction to the excited electron and hole is described by the HSE functional. One obtains the so-called quasiparticle gap. The quasiparticle effects lead to a gap increase of approximately 1 eV with respect to the DFT-LDA gap. Unfortunately, the hybrid-functional computations are limited to $Sn_{41}H_{60}$ nanocrystals, i.e., to about 100 atoms in a supercell. Larger nanocrystals, e.g., $Sn_{525}H_{372}$, cannot be treated together with spin-orbit interaction despite the freezing of Sn 4*d* electrons into the core. Using the ΔSCF method as described in Sec. II, both excitonic effects as well as quasiparticle effects are included. One obtains the so-called optical gaps. However, Fig. 9 shows that the differences between the ΔSCF excitation energies and the KS gaps from DFT-LDA calculations are smaller than 30 meV for all NCs with more than one tin atom. Hence, there seems to be a cancellation of excitonic and quasiparticle effects in the hydrogenated Sn NCs. This fact seems to be a general observation for nanostructures.[44,79] Similar results were reported for Si, Ge, SnTe, PbSe, and PbTe nanodots.[5,44,72,80] In case of SnTe, PbSe, and PbTe nanodots, the underestimation of the excitation energy identified with the KS gaps compared to the results of the ΔSCF method amounts up to 50 meV,[72,80] which is in the same order of magnitude as our findings.

D. Topological transition

The monotonous decrease of the fundamental gaps with increasing NC diameter as shown in Figs. 6 and 9 suggests that the gap shrinks in such a way that the band inversion between the LUMO levels transforming as atomlike *s* levels and the HOMO levels transforming like atomlike *p* levels may happen in agreement with the findings for bulk α-tin (see Sec. III B). In Sec. III B it was shown that in the bulk case the *s*-like Γ_{6c} level lies below the *p*-like Γ_{8v} state. Since the ordering in case of the nanocrystals is inverted with respect to the bulk as discussed above in this section, and the gap decreases with increasing NC size, there must be a topological transition for increasing NC diameter where the energetic level ordering of the Γ_{6c} and Γ_{8v} states is interchanged.

As it is computationally too expensive to investigate this topological transition by *ab initio* calculations, we fit the energetic HOMO and LUMO positions to an inverse diameter dependence such that for infinite diameter the negative bulk band gap is reproduced [cf. Fig. 10(a)]. As shown in Fig. 7 for $Sn_{17}H_{36}$ the HOMO (LUMO) levels possess Γ_{8v} (Γ_{6c}) character. The spin-orbit split-off HOMO state with bulk Γ_{7v} symmetry is displayed for comparison. We found the crossing of HOMO and LUMO states to occur around 11.46 nm. For comparison the corresponding TB results are plotted in Fig. 10(b). NCs up to 19 335 Sn atoms and 4092 H atoms are investigated. The TB results for the diameter for level crossing is 12.7 nm as displayed in Fig. 10(b) which is in very good agreement to the *ab initio* value. However, the identification of the transition within TB is difficult due to the problem of identification of the symmetry character of

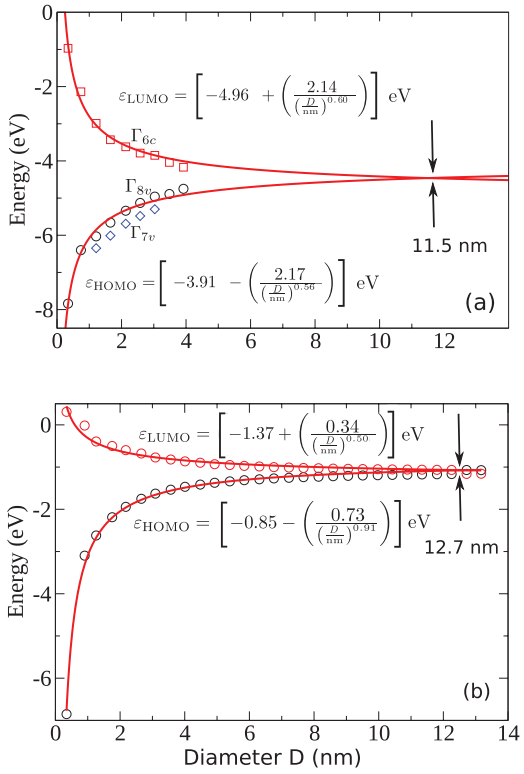

FIG. 10. (Color online) Diameter dependence of the HOMO and LUMO level positions are plotted. The respective bulk orbital symmetries Γ_{6c} and Γ_{8v} are indicated. In addition, the energy position of the first occupied state below the HOMO with Γ_{7v} symmetry is also given. (a) The KS eigenvalues from the DFT-LDA calculation with SOC. The vacuum level of the electrostatic potentials is used as energy zero. (b) Eigenvalues derived from the diagonalization of the TB Hamiltonian using the parameters listed in Table III.

the HOMO and LUMO states. Therefore, we have fitted the diameter dependence similar as for the *ab initio* values and identified the critical diameter as the crossing value of the fit curves for the two levels. The slightly larger diameter found within the TB approximation is a consequence of a fit of the TB parameters to the HSE06 band structure of α-tin. As shown in Fig. 9 the HSE values for the pair excitation energies are slightly larger than the LDA ones and, hence, result in a level crossing at somewhat larger diameters.

V. SUMMARY AND CONCLUSIONS

We have presented results of *ab initio* calculations for structural, energetic, and electronic properties of α-tin and its hydrogenated nanocrystals up to $Sn_{525}H_{372}$. The spin-orbit interaction is taken into account. The influence of many-body effects on the band ordering and energy gaps have been studied in detail. The bulk quasiparticle band structure of α-tin has been used to derive a first-nearest-neighbor tight-binding model Hamiltonian with a sp^3s^* basis set and SOC. It has been applied to compute the electronic energy levels also for big NCs up to a diameter of about 13 nm, i.e., $Sn_{19335}H_{4092}$. Structural relaxation of tedrahedrally bonded NCs with a hydrogen passivation of the dangling bonds showed that the spatial rearrangement is more significant for smaller dots while the geometry

of the biggest NCs is less influenced with respect to the bulk. The starting T_d symmetry is conserved. The Sn-Sn bonds in the core of the NCs tend to elongation while the bonds closer to the NC surface are shrinked. The formation and energetic stability of hydrogenated Sn NCs depends on the NC diameter and the preparation conditions. There is a general tendency for an energetic favorization of larger NCs under equilibrium conditions.

Comparing the electronic structure of the bulk zero-gap semiconductor to those of the NCs we observe an inversion in the ordering of states transforming similar to s and p states above and below the Fermi level. Calculating the size dependence of the HOMO-LUMO gaps, we found a decreasing spatial confinement causing a decrease of the gaps with rising diameter. Consequently, a topological transition where the level ordering changes for a certain NC size is predicted. Fitting the diameter dependence of the energetic position of HOMO and LUMO states in DFT-LDA, we determine the NC diameter for the topological transition to be approximately 11.5 nm, which fits quite well to the result 12.7 nm obtained from the calculations in tight-binding approximation.

The lowest two-particle excitation energies have been studied within different approximations for the electron-electron interaction, in order to distinguish between quasiparticle and optical gap. We found that there is an almost cancellation of quasiparticle and excitonic effects which is in agreement to previous calculations for NCs made for other materials. Consequently, the differences of Kohn-Sham eigenvalues for HOMO and LUMO already give a reasonable description of the optical gaps.

ACKNOWLEDGMENTS

We gratefully acknowledge financial support of the Austrian Fond zur Förderung der Wissenschaftlichen Forschung in the framework of SFB 25 Infrared Optical Nanostructures. L.M. thanks the Carl-Zeiss Foundation for a scholarship. The computations have been performed in part using the facilities of the John von Neumann Institute for Computing in Jülich.

TABLE III. First-nearest-neighbor TB parameters for α-Sn in an orthogonal sp^3s^* model including spin-orbit interaction with a coupling constant of $\Delta_0 = 0.68$ eV. The values are given in the notation of Slater and Koster[81] and compared to those of Vogl *et al.*[28] All values are in eV.

Parameter	This work	Ref. 28
E_s	−7.2029	−5.8700
E_p	0.0032	1.3300
E_{s^*}	14.1081	5.9000
$V_{ss\sigma}$	−1.4802	−1.4175
$V_{s^*s^*\sigma}$	0.4795	–
$V_{sp\sigma}$	1.9034	1.9536
$V_{s^*p\sigma}$	2.7564	2.5522
$V_{pp\sigma}$	3.3555	2.3725
$V_{pp\pi}$	−1.6848	−0.6870

APPENDIX: TIGHT-BINDING PARAMETERS FOR α-SN

The HSE + SOC band structure in Fig. 2, more precisely, 14 of their eigenvalues at the high-symmetry points, five at Γ, three at X, and six at L are used to fit the first-nearest-neighbor TB parameters. A basis set of eight (with spin) sp^3s^* orbitals is applied. The three diagonal intra-atomic matrix elements E_s, E_p, and E_{s^*} as well as seven interatomic two-center integrals are taken into account. The interaction between s and s^* orbitals is neglected. Three-center integrals of p orbitals are approximated by a constant $A = 1.995$ eV. Spin-orbit interaction is described by one intra-atomic parameter chosen as $\Delta_0 = 0.68$ eV. The resulting TB parameters are listed in Table III. The on-site matrix elements E_s, E_p, and E_{s^*} are chosen in such a way that the zero of energy is at the Γ_8 valence band. Despite the neglect of SOC and ss^* interaction in Ref. 28 the obtained matrix elements are similar as that predicted by Vogl *et al.* Only the s^* energy value is much larger in our fit. However, such large s^* energies have been also found for HgTe.[27]

*sebastian.kuefner@uni-jena.de

[1] A. Alivisatos, Science **271**, 933 (1996).
[2] T. Martin, Phys. Rep. **273**, 199 (1996).
[3] Y. Yin and A. P. Alivisatos, Nature (London) **437**, 664 (2005).
[4] M. A. van Huis, N. P. Young, G. Pandraud, J. F. Creemer, D. Vanmaekelbergh, A. I. Kirkland, and H. W. Zandbergen, Adv. Mater. **21**, 4992 (2009).
[5] K. Seino *et al.*, Nanotechnology **20**, 135702 (2009).
[6] I. Tsidilkowski, *Gapless Semiconductors—A New Class of Materials* (Akademie, Berlin, 1988).
[7] J. R. Chelikowsky and M. L. Cohen, Phys. Rev. B **14**, 556 (1976).
[8] R. V. S. Jensen, T. Garm Pedersen, and K. Pedersen, Phys. Status Solidi C **8**, 1002 (2011).
[9] A. Rogach, S. V. Kershaw, M. Burt, M. T. Harrison, A. Kornowski, A. Eychmller, and H. Weller, Adv. Mater. **11**, 552 (1999).
[10] M. V. Kovalenko, E. Kaufmann, D. Pachinger, J. Roither, M. Huber, J. Stangl, G. Hesser, F. Schäffler, and W. Heiss, J. Am. Chem. Soc. **128**, 3516 (2006).
[11] H.-C. Weissker, J. Furthmüller, and F. Bechstedt, Phys. Rev. Lett. **90**, 085501 (2003).
[12] K. Seino, F. Bechstedt, and P. Kroll, Phys. Rev. B **82**, 085320 (2010).
[13] L. E. Ramos, J. Paier, G. Kresse, and F. Bechstedt, Phys. Rev. B **78**, 195423 (2008).
[14] W. G. Burgers and L. J. Groen, Discuss. Faraday Soc. **23**, 183 (1957).
[15] S. Takatani and Y. W. Chung, Phys. Rev. B **31**, 2290 (1985).
[16] H. Landolt and R. Börnstein, *Zahlenwerte und Funktionen aus Physik, Chemie, Astronomie, Geophysik und Technik* (Springer, Berlin, 1982), Vol. 6.
[17] S. Huang, E.-C. Cho, G. Conibeer, M. A. Green, D. Bellet, E. Bellet-Amalric, and S. Cheng, J. Appl. Phys. **102**, 114304 (2007).
[18] S. Huang, Y. H. So, G. Conibeer, and M. A. Green, J. Appl. Phys. **105**, 124303 (2009).
[19] M. F. Fyhn, J. Chevallier, A. Nylandsted Larsen, R. Feidenhans'l, and M. Seibt, Phys. Rev. B **60**, 5770 (1999).

[20]I. Arslan, T. J. V. Yates, N. Browning, and P. A. Midgley, Science **309**, 2195 (2005).
[21]R. Ragan and H. Atwater, Appl. Phys. A **80**, 1335 (2005).
[22]Y. Lei, P. Mock, T. Topuria, N. D. Browning, R. Ragan, K. S. Min, and H. A. Atwater, Appl. Phys. Lett. **82**, 4262 (2003).
[23]M. Z. Hasan and C. L. Kane, Rev. Mod. Phys. **82**, 3045 (2010).
[24]J. E. Moore, Nature (London) **464**, 194 (2010).
[25]J. Vidal, X. Zhang, V. Stevanović, J.-W. Luo, and A. Zunger, Phys. Rev. B **86**, 075316 (2012).
[26]P. Moontragoon, N. Vukmirovic, Z. Ikonic, and P. Harrison, J. Appl. Phys. **103**, 103712 (2008).
[27]G. Allan and C. Delerue, Phys. Rev. B **86**, 165437 (2012).
[28]P. Vogl, H. P. Hjalmarson, and J. D. Dow, J. Phys. Chem. Solids **44**, 365 (1983).
[29]P. Hohenberg and W. Kohn, Phys. Rev. **136**, B864 (1964).
[30]W. Kohn and L. J. Sham, Phys. Rev. **140**, A1133 (1965).
[31]G. Kresse and J. Furthmüller, Phys. Rev. B **54**, 11169 (1996).
[32]G. Kresse and J. Furthmüller, Comput. Mater. Sci. **6**, 15 (1996).
[33]D. M. Ceperley and B. J. Alder, Phys. Rev. Lett. **45**, 566 (1980).
[34]J. P. Perdew and A. Zunger, Phys. Rev. B **23**, 5048 (1981).
[35]J. P. Perdew, J. A. Chevary, S. H. Vosko, K. A. Jackson, M. R. Pederson, D. J. Singh, and C. Fiolhais, Phys. Rev. B **46**, 6671 (1992).
[36]J. P. Perdew and Y. Wang, Phys. Rev. B **33**, 8800 (1986).
[37]J. P. Perdew, K. Burke, and M. Ernzerhof, Phys. Rev. Lett. **77**, 3865 (1996).
[38]S. L. Dudarev, G. A. Botton, S. Y. Savrasov, C. J. Humphreys, and A. P. Sutton, Phys. Rev. B **57**, 1505 (1998).
[39]J. Heyd, G. E. Scuseria, and M. Ernzerhof, J. Chem. Phys. **118**, 8207 (2003).
[40]W. G. Aulbur, L. Jönsson, and J. W. Wilkins, in *Advances in Research and Applications*, Solid State Physics, Vol. 54, edited by H. Ehrenreich and F. Spaepen (Academic, New York, 1999), pp. 1–218.
[41]R. O. Jones and O. Gunnarsson, Rev. Mod. Phys. **61**, 689 (1989).
[42]S. Öğüt, J. R. Chelikowsky, and S. G. Louie, Phys. Rev. Lett. **79**, 1770 (1997).
[43]R. W. Godby and I. D. White, Phys. Rev. Lett. **80**, 3161 (1998).
[44]H.-C. Weissker, J. Furthmüller, and F. Bechstedt, Phys. Rev. B **65**, 155328 (2002).
[45]P. E. Blöchl, Phys. Rev. B **50**, 17953 (1994).
[46]G. Kresse and D. Joubert, Phys. Rev. B **59**, 1758 (1999).
[47]D. Hobbs, G. Kresse, and J. Hafner, Phys. Rev. B **62**, 11556 (2000).
[48]H. J. Monkhorst and J. D. Pack, Phys. Rev. B **13**, 5188 (1976).
[49]C. Jo and K. Lee, J. Chem. Phys. **113**, 7268 (2000).
[50]B. Akdim, D. A. Papaconstantopoulos, and M. J. Mehl, Philos. Mag. B **82**, 47 (2002).
[51]T. G. Pedersen, C. Fisker, and R. V. Jensen, J. Phys. Chem. Solids **71**, 18 (2010).
[52]Y. Li and P. J. Lin-Chung, Phys. Rev. B **27**, 3465 (1983).
[53]D. J. Chadi, Phys. Rev. B **16**, 790 (1977).
[54]T. B. Boykin, Phys. Rev. B **57**, 1620 (1998).
[55]R. Farrow, D. Robertson, G. Williams, A. Cullis, G. Jones, I. Young, and P. Dennis, J. Cryst. Growth **54**, 507 (1981).
[56]A. Thewlis, J. Davey, Nature (London) **174**, 1011 (1954).
[57]S. Groves and W. Paul, Phys. Rev. Lett. **11**, 194 (1963).
[58]W. Harrison, *Electronic Structure and the Properties of Solids* (Dover, New York, 1989).
[59]L. Schimka, J. Harl, and G. Kresse, J. Chem. Phys. **134**, 024116 (2011).
[60]A. Dal Corso, Phys. Rev. B **86**, 085135 (2012).
[61]R. Poerschke and O. Madelung, *Data in Science and Technology, Semiconductors Group IV Elements and III-V Compounds* (Springer, Berlin, 1991).
[62]F. H. Pollak, M. Cardona, C. W. Higginbotham, F. Herman, and J. P. Van Dyke, Phys. Rev. B **2**, 352 (1970).
[63]M. Cardona, K. L. Shaklee, and F. H. Pollak, Phys. Rev. **154**, 696 (1967).
[64]S. Bloom and T. Bergstresser, Solid State Commun. **6**, 465 (1968).
[65]M. van Schilfgaarde (private communication).
[66]K. Hummer (unpublished).
[67]S.-H. Wei and A. Zunger, Phys. Rev. B **37**, 8958 (1988).
[68]J. Furthmüller, P. H. Hahn, F. Fuchs, and F. Bechstedt, Phys. Rev. B **72**, 205106 (2005).
[69]L. E. Ramos, J. Furthmüller, and F. Bechstedt, Phys. Rev. B **72**, 045351 (2005).
[70]Sargent-Welch, *Table of Periodic Properties of the Elements* (Sargent-Welch Scientific, Skokie, IL, 1980).
[71]J.-W. Luo, S.-S. Li, J.-B. Xia, and L.-W. Wang, Appl. Phys. Lett. **88**, 143108 (2006).
[72]L. E. Ramos, H.-C. Weissker, J. Furthmüller, and F. Bechstedt, Phys. Status Solidi B **242**, 3053 (2005).
[73]L. Landau and E. Lifshitz, *Statistical Physics* (Pergamon, Oxford, 1959), Vol. 5.
[74]F. Trani, G. Cantele, D. Ninno, and G. Iadonisi, Phys. Rev. B **72**, 075423 (2005).
[75]H. Fu, L.-W. Wang, and A. Zunger, Phys. Rev. B **57**, 9971 (1998).
[76]R. Enderlein and N. Horring, *Fundamentals of Semiconductor Physics and Devices* (World Scientific, Singapore, 1997).
[77]F. Fuchs, J. Furthmüller, F. Bechstedt, M. Shishkin, and G. Kresse, Phys. Rev. B **76**, 115109 (2007).
[78]F. Bechstedt, F. Fuchs, and G. Kresse, Phys. Status Solidi B **246**, 1877 (2009).
[79]C. Delerue, M. Lannoo, and G. Allan, Phys. Rev. Lett. **84**, 2457 (2000).
[80]R. Leitsmann and F. Bechstedt, ACS Nano **3**, 3505 (2009).
[81]J. C. Slater and G. F. Koster, Phys. Rev. **94**, 1498 (1954).